Available online at www.sciencedirect.com
ScienceDirect
Bioorganic & Medicinal Chemistry Letters 18 (2008) 2990–2995
Bioorganic & Medicinal Chemistry Letters

Fragment-based discovery of hepatitis C virus NS5b RNA polymerase inhibitors

Stephen S. Antonysamy,[a] Brandon Aubol,[a] Jeff Blaney,[a] Michelle F. Browner,[b] Anthony M. Giannetti,[b] Seth F. Harris,[b] Normand Hébert,[a,*] Jörg Hendle,[a] Stephanie Hopkins,[a] Elizabeth Jefferson,[a] Charles Kissinger,[a] Vincent Leveque,[b] David Marciano,[a] Ethel McGee,[a] Isabel Nájera,[b] Brian Nolan,[a] Masaki Tomimoto,[a] Eduardo Torres[a] and Tobi Wright[a]

[a]*Medicinal Chemistry, SGX Pharmaceuticals, Inc., 10505 Roselle Street, San Diego, CA 92121, USA*
[b]*Roche Palo Alto, 3431 Hillview Avenue, Palo Alto, CA 94304, USA*

Received 21 December 2007; revised 14 March 2008; accepted 18 March 2008
Available online 22 March 2008

Abstract—Non-nucleoside inhibitors of HCV NS5b RNA polymerase were discovered by a fragment-based lead discovery approach, beginning with crystallographic fragment screening. The NS5b binding affinity and biochemical activity of fragment hits and inhibitors was determined by surface plasmon resonance (Biacore) and an enzyme inhibition assay, respectively. Crystallographic fragment screening hits with ~1–10 mM binding affinity (K_D) were iteratively optimized to give leads with ~200 nM biochemical activity and low μM cellular activity in a Replicon assay.

Hepatitis C virus is the leading cause of chronic liver disease throughout the world. Patients infected with HCV are at risk of developing cirrhosis of the liver and subsequent hepatocellular carcinoma, and hence HCV is one of the major reasons for liver transplantation. HCV NS5b polymerase has been the focus of many drug discovery efforts,[1] but has proven to be a difficult target as evidenced by the small number of clinical candidates targeting this enzyme to date.[2]

Fragment-based lead discovery has been recently reviewed.[3] Crystallographic fragment-based screening seemed particularly well suited for a challenging target such as HCV polymerase, since previous work has shown that the high screening hit rate for such small, low MW compounds can often identify novel, tractable hits that can be optimized into potent leads with good 'drug-like' properties.[4] In particular, crystallographic fragment screening can identify hits that may be too weak to be identified in biochemical assays. Crystallographic fragment screening also provides unambiguous proof of binding to the target site and reveals the details of the hits binding mode, providing clear direction for how they may be optimized into more potent lead compounds. Cocrystal structures of HCV NS5b RNA dependent RNA polymerase (NS5b) with small molecule inhibitors have been previously reported.[5] We developed experimental protocols for growing NS5b crystals that were suitable for determining inhibitor cocrystal structures by soaking.

Fragments in the screening library were chosen to be consistent with 'lead-like' properties,[6] and also to include two or more substituents to facilitate analog synthesis. The fragment library had a MW range of 100–220D and an average MW of 160.[7] About half of the fragments contain an aromatic bromine, both as a convenient substituent for synthesis and to facilitate determination of bound hits by collecting X-ray data at the bromine anomalous dispersion wavelength. Ninety-six mixtures of 10 fragments (5 mM concentration each) were incubated with the NS5b protein crystals for 24 h. Datasets were obtained for 89 of 96 mixtures at a typical resolution of 1.7 Å (range 1.6–2.1 Å). Twenty individual hits were identified, 17 of which were bound

Keywords: HCV; NS5b; Fragment screening; Protein crystallography.
* Corresponding author. Tel.: +1 858 558 4850; fax: +1 858 558 0642; e-mail: nhebert@sgxpharma.com

0960-894X/$ - see front matter © 2008 Elsevier Ltd. All rights reserved.
doi:10.1016/j.bmcl.2008.03.056

at an allosteric site in the thumb domain.[8] In most cases the hit was unambiguously identified directly from the mixture screen. Other hits with less well-defined electron density were identified by soaking the individual compounds from the mixture.

Surface Plasmon Resonance (SPR) technology as implemented with BIAcore instruments was applied initially to detect protein–protein interactions, followed by protein–ligand interactions with high affinity (e.g., sub-μM). Recent hardware and software improvements have enabled the determination of binding affinities of smaller, weaker ligands, such that SPR analysis can be used to detect fragment binding. Using this technique we were able to measure equilibrium binding affinities (K_D) for fragments and elaborated molecules with modest affinity.

The fragments found to bind to the thumb site had a number of common features (Fig. 1), most notably the frequent presence of an aryl or heteroaryl bromide, and a preponderance of carboxylic acids. The hits tolerated a range of substituents meta and para to the bromine. Interestingly, the corresponding chloro substituted analogs were not observed crystallographically.

A number of hits were observed to interact with the carboxylic acid binding site (S476 and Y477) in a manner analogous to the published Shire inhibitor **6**.[9,10] For example, **5** is involved in two hydrogen bonds to S476 and Y477 backbone NHs. These interactions were also observed with other carboxylic acids. In the case of **2**, the carboxylic acid binds to S476 and Y477 while the bromophenyl occupies a hydrophobic pocket in the floor of the binding site. In a biochemical assay, which measures the inhibition of ^{3}H UTP incorporation into RNA using a poly A RNA template,[11] the IC_{50} value of fragments discovered in the crystallographic screen was in the 200–500 μM range, or was too weak to be measured. The binding affinity of **1** and **4** to the NB5b protein was in the millimolar range.[12]

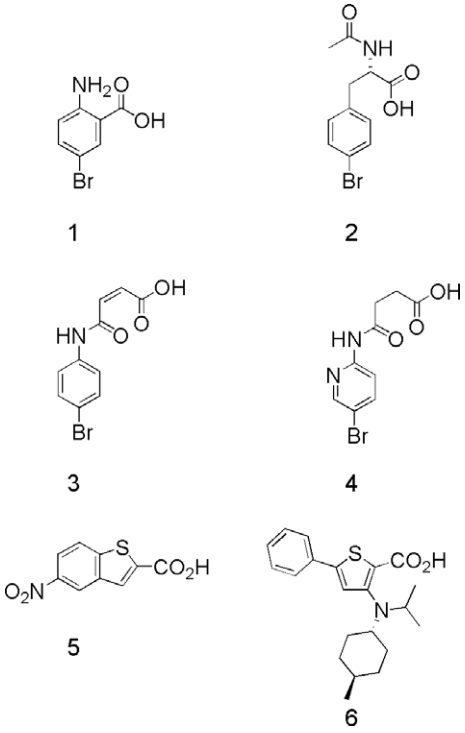

Figure 1. Some of the fragment hits observed at Thumb site in NS5b crystal structures, and Reference inhibitor **6** from reference 2.

In parallel, the biochemical assay was used to identify hits from the same fragment library screened at high concentration. None of the biochemical hits, which had IC_{50} values ranging from 2 to >100 μM, were observed to bind to the NS5b protein crystals in soaking experiments. SPR analysis of the biochemical hits also failed to detect any binding affinity.

The initial optimization efforts were focused on **1** which offered a number of possibilities for elaboration. The goal was to increase the affinity and biochemical activity by creating additional interactions in the binding pocket between R501 and S476 and Y477 (Fig. 2).

A second class of fragments was also discovered in the initial crystallographic fragment screen (**3** and **4** are representative examples). In this case, the bromoaryl moiety binds in the pocket as in **1**, but the amide carbonyl oxygen interacts with the S476 backbone NH in the carboxylic acid binding site. The succinic acid electron density is well defined, with the carboxylate interacting with the S476 hydroxyl on the surface of the protein. Since this is a surface residue, it was unclear how much binding affinity was due to this interaction and whether it was critical for binding. An initial library of anthranilamides **7** was made using a diverse selection of primary, secondary, and aromatic amines (Scheme 1). A second set of amines, distinct from the first, was selected and coupled to 5-bromo anthranilic acid **1**, and then treated with succinic anhydride to give the succinamide products **8** (Scheme 1).

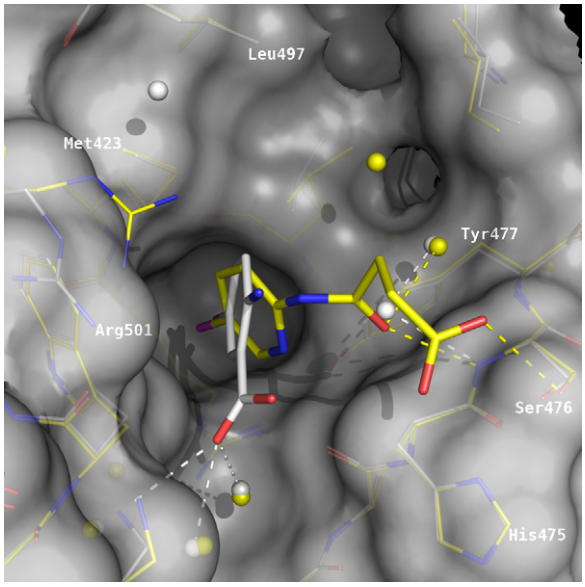

Figure 2. Crystal structure of fragments **1** and **4** bound to NS5B.

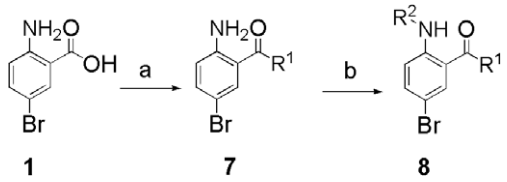

Scheme 1. Reagents and condition: (a) **1**, R^1 Amine (1.2 equiv), HATU (1.2 equiv), DIEA (1.2 equiv), DMF; (b) Succinic anhydride (1.2 equiv) Toluene, 90 °C.

The initial set of compounds was screened and a number of derivatives showed biochemical inhibition in the 17–500 μM range, with comparable SPR binding affinities (Table 1). From this initial screening set, it was clear that secondary amides were less active than tertiary, and that cyclic amides were preferred over acyclic amides. The measured binding affinities were generally in agreement with the biochemical results. SPR analysis also allowed us to identify and exclude compounds that displayed non-ideal behavior such as aggregation, poor solubility, or non-stoichiometric binding, which was presumed to reflect non-specific inhibition (e.g., **7b** and **7c**).

Table 1. RNA polymerase inhibition of 5-bromoanthranilic acid derivatives

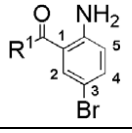

Compound	R^1	IC_{50} (μM)	KD (μM)
7a	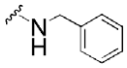	>500	nd
7b	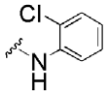	178	nd
7c	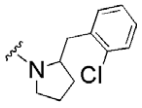	57	ins
7d	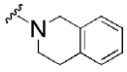	132	210
7e	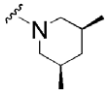	17	14
7f	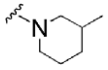	170	192
7g		>500	nd
7h		>500	nd
7i	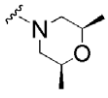	190	36
7j		>500	nd

Values are means of duplicate experiments. K_D was measured by Biacore. Standard deviations are ±50% of the reported values.

Based on these initial results, we prepared additional analogs of **7** to probe the binding site further. An expanded set of R^1, including substituted pyrrolidines, piperidines, piperazines, and azepines, as well as bicyclic amines, was coupled to 5-bromoanthranilic acid **1**. The second set of compounds retained the most active 3,5-*cis*-dimethylpiperidine at R^1, coupled to a series of 5- and 6-substituted 3-bromo or 3-chlorobenzoic acids. These were designed to probe the steric and electronic preferences in the hydrophobic pocket, as well as attempting to extend into the groove. Biochemical screening of these second round arrays revealed no compounds with greater inhibition than compound **7e**.

Additional analogs of **7e** with substitution ortho to the aniline provided other insights. A number of small substituents were tolerated in crystal structures (Cl, CH_3) but all were less potent than **7e**. To provide insight for this lack of improvement, a number of compounds were soaked into NS5b crystals. These crystal structures showed that the 3,5-dimethylpiperidine amide makes a number of critical interactions with the protein. The amide carbonyl is twisted out of the plane of the aryl group and interacts with the guanidine of R501 (Fig. 3). Both methyl groups on the piperidine appear to be necessary, since removing one or both methyls (e.g., **7f** and **7g**) reduces activity. The dimethyl piperidine also seems to have optimal interactions with the floor of the binding site, since no other amines profiled, including substituted morpholines and thiomorpholines, offered any improvement. Pyrrolidines, tetrahydroisoquinolines, azepines, and piperazines also did not improve activity beyond **7e**. Crystal structures reveal that although several pyrrolidine derivatives (e.g., **7c**) bind to the site, their binding mode is different from **7e**. In these compounds, the amide carbonyl oxygen no longer

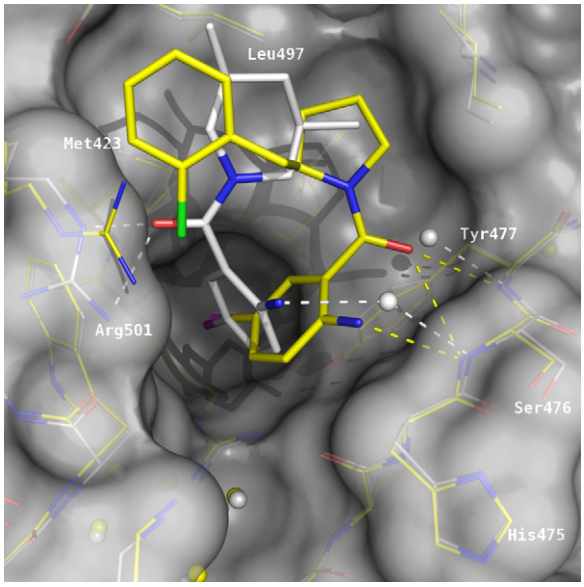

Figure 3. Crystal structures of **7c** and **7e** bound to NS5b.

interacts with R501, but rather hydrogen bonds to the backbone NH of S476. In this conformation, there is a large portion of the site unfilled. In compounds with a substituent ortho to the aniline, the aromatic ring rotates to accommodate the substituent. This prevents the ring from pushing down into the pocket to the same extent as the unsubstituted analogs.

Table 2. RNA polymerase inhibition of succinate derivatives

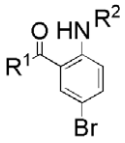

Compound	R^1	R^2	IC_{50} (μM)	K_D (μM)
8a	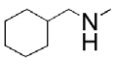	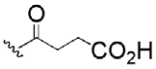	>500	nd
8b		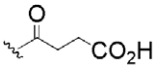	>500	nd
8c		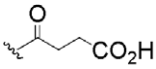	533	nd
8e		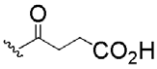	1.0	0.31
8f			11	1.7
8g		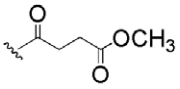	2.1	ins
8h		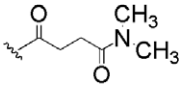	0.4	0.30
8i		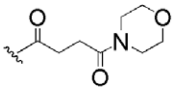	0.25	0.46
8j		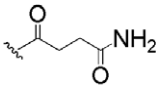	4.3	9.4
8k		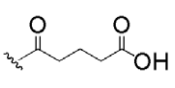	9	nd
8l		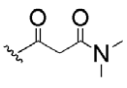	11	nd
8m	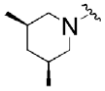		7.5	nd

Values are means of duplicate experiments. K_D were measured by Biacore. Standard deviations are ±50% of the reported values.
ND, not determined; Ins, insoluble.

As can be seen in Table 2, incorporation of the succinic acid group into the preferred compound **7e** to provide compound **8e** showed a 17-fold improvement over the parent, and was found to maintain the interactions of the succinamide fragment **4**. Interestingly, introduction of the succinate into other anthranilamides (e.g., **8a**–**c**) led to a marked decrease in biochemical activity. We therefore focused on determining which of the interactions made by the succinamide moiety were responsible for the gain in potency in going from **7e** to **8e**.

Truncation of the terminal acid and replacement with an acetamide or sulfonamide (**8f** and **8m**), or ester formation (**8g**) were found to be deleterious. Various amides were also tested. The dimethyl amide **8h** and the morpholine amide **8i** were 2.5- and 4-fold more active than the carboxylic acid, respectively. Examination of the cocrystal structures of acid **8e** (Fig. 4) showed that the carbonyl adjacent to the aniline nitrogen interacts with the backbone NH of S476 as in fragment **4**, while the carboxylic acid binds to the S476 hydroxyl and the imidazole of H475. In the case of the morpholine amide **8i**, the interaction of the anilide carbonyl with S476 was unchanged, but the morpholine stacks with the imidazole ring instead of forming a hydrogen bond. The primary amide **8j** was 18-fold less active than the morpholine amide **8i**. A 1,4-dicarbonyl arrangement appears to be preferred, since glutarate **8k** and malonamide **8l** were both 10-fold weaker than parent **8e**. It is likely that a 1 or 3 atom linker between the carbonyls does not allow the terminal group to interact productively with S476 and H475.

At this point we focused our efforts in three directions: first, optimizing the stacking interaction with H475; second, reducing the rotational freedom of the succinate moiety; and third, exploring other 1,4-dicarbonyl arrangements.

Starting from **7e**, ketoamides such as **9a**–**c** were obtained by acylation of the aniline (Scheme 2). The results

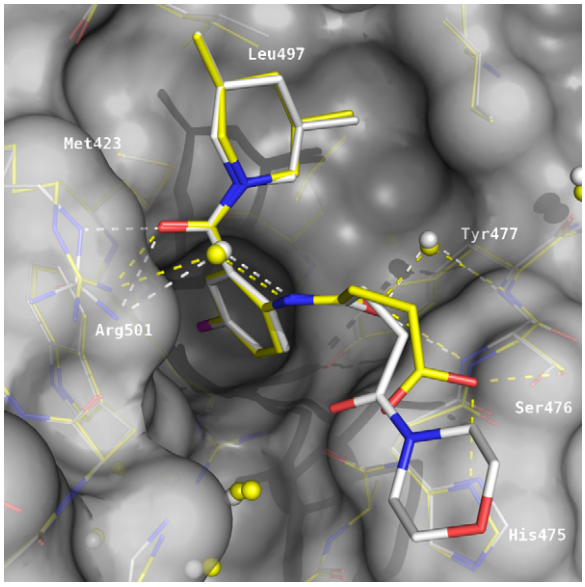

Figure 4. Crystal structure of **8e** and **8i** bound to NS5b.

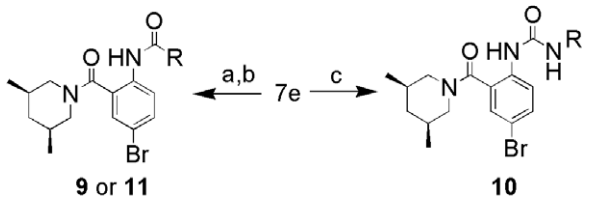

Scheme 2. Reagents: (a) **7e**, RCOOH (1.2 equiv), HATU (1.2 equiv), DIEA (1.2 equiv), DCM/DMF; (b) TFA/DCM, then, RCOOH (1.2 equiv), HATU (1.2 equiv), DIEA (1.2 equiv), DCM/DMF; (c) COCl2, DCM, NaHCO3, then, RNH2.

showed that the terminal amide could be replaced with an aryl ketone, and provide similar biochemical activity (Table 3).

Replacement of C2 of the succinate with nitrogen maintained potency as can be seen comparing the urea derivative **10a** with its direct analog **8h**. Interestingly, compounds such as **10b–d**, which replaced the terminal amide with an aromatic or heteroaromatic ring were also active, indicating that the carbonyl is not essential, but can be replaced by another group capable of π stacking with the H475. The results of compounds **9** and **10** are consistent with the notion that the stacking interaction with H475 is providing increased activity, and that this is possible with a range of different substituents. Since these interactions occur in a solvent exposed region there is little steric discrimination to prevent groups differing widely in size from binding efficiently. As can be seen in the urea series, both electron-rich and electron-poor rings interact favorably in this region.

Inspired by the positive results with **9** and **10**, a series of amino acid amide derivatives (**11a–e**) were also prepared. Glycine derivatives **11a–c**, which replaces a carbon in **9** with nitrogen, showed similar biochemical potencies as well as binding affinities. Of the many cyclic analogs prepared (not shown), only proline analogs such as **11d** and **11e** exhibited less than 10 μM potency. These observations indicate that analogs with restricted rotation between the carbonyl moieties derived their potency from a dependency on the conformation of the side chain.

Based on both biochemical activity and binding affinity, a set of compounds was selected for testing in the Replicon assay (Table 4). Compounds with non-ideal behavior in the SPR assay were discarded.

The most active was the proline analog **11e**, possessing an EC_{50} of 3.7 μM. The correlation of the replicon activity of these analogs with the SPR affinity and with the biochemical activity is observed, although there are outliers in both cases. Nonetheless, both assays taken together were good predictors of Replicon activity. Interestingly, these results demonstrate that compounds without a charged group can interact strongly with the carboxylic acid binding site, S476 and Y477.

In summary, this work demonstrates that fragments with millimolar binding affinity discovered by crystallographic screening can be improved over 1000-fold resulting in compounds with nanomolar affinity using structure-based design. SPR analysis, using BIAcore technology, was critical in the early stages of this work, as most of the initial fragments showed undetectable

Table 3. RNA polymerase inhibition of succinate derivatives

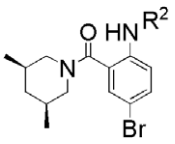

Compound	R^2	IC_{50} (μM)	KD (μM)
9a	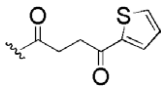	0.44	0.97
9b	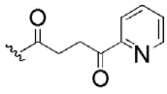	0.54	1.85
9c	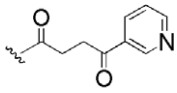	0.59	1.04
10a	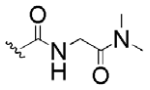	0.60	0.46
10b	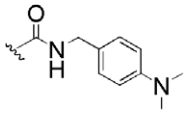	1.0	0.80
10c	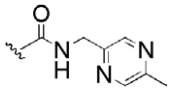	0.36	0.35
10d	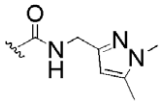	0.17	0.37
11a	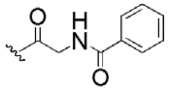	0.13	0.54
11b	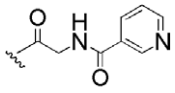	0.43	0.57
11c	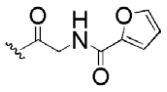	0.25	1.02
11d	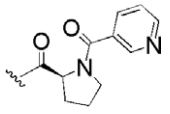	0.35	1.28
11e	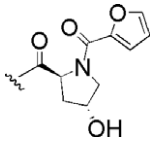	1.03	0.15

Values are means of duplicate experiments. K_D were measured by Biacore. Standard deviations are ±50% of the reported values.

Table 4. Replicon activity for selected analogs

Compound	Replicon activity EC_{50} (μM)
8e	22.8 ± 1.5
8h	6.1 ± 1.0
8i	7.4 ± 1.6
9a	4.3 ± 0.3
9c	7.9 ± 0.4
10a	5.6 ± 0.5
10b	4.9 ± 0.7
10c	6.9 ± 0.6
10d	4.6 ± 0.9
11a	5.5 ± 0.4
11b	5.7 ± 0.7
11c	8.7 ± 0.1
11d	12.9 ± 2.9
11e	3.7 ± 0.2

Values are the mean of at least $n = 2$ experiments.

biochemical activity. SPR analysis also helped diagnose biochemical false positives during fragment optimization; several of these analogs did not bind to the enzyme based on both SPR and crystallographic analysis. Using these tools, neutral inhibitors of NS5b were discovered and shown to possess interesting cellular activity. Further progress on this series will be reported in due course.

Acknowledgments

We gratefully acknowledge the support of Roche Palo Alto, Dr. David Myszka of the University of Utah, Dr. John Cashman of the Human Biomolecular Research Institute, San Diego, CA.

References and notes

1. Gordon, C. P.; Keller, P. A. *J. Med. Chem.* **2005**, *48*, 1; Tan, S.-L.; Pause, A.; Shi, Y.; Sonenberg, N. *Nat. Rev. Drug Disc.* **2002**, *1*, 867.
2. Hirashima, S.; Suzuki, T.; Ishida, T.; Noji, S.; Yata, S.; Ando, I.; Komatsu, M.; Ikeda, S.; Hashimoto, H. *J. Med. Chem.* **2006**, *49*, 4721.
3. Erlanson, D. A.; McDowell, R. S.; O'Brien, T. *J. Med. Chem.* **2004**, *47*, 3463; Hartshorn, M. J.; Murray, C. W.; Cleasby, A.; Frederickson, M.; Tickle, I. J.; Jhoti, H. *J. Med. Chem.* **2005**, *48*, 430; Hajduk, P. J.; Greer, J. *Nat. Rev. Drug Disc.* **2007**, *6*, 211.
4. Nienaber, V. L.; Richardson, P. L.; Klighofer, V.; Bouska, J. J.; Giranda, V. L.; Greer, J. *Nat. Biotechnol.* **2000**, *18*, 1105; Rees, D. C.; Congreve, M.; Murray, C. W.; Carr, R. *Nat. Rev. Drug Disc.* **2004**, *3*, 660.
5. The PDB ID codes for complexes discussed in this paper are: 3CIZ, 3CJ0, 3CJ2, 3CJ3, 3CJ4, 3CJ5.
6. Schuffenhausen, A.; Ruedisser, S.; Marzinzik, A. L.; Jahnke, W.; Blommers, M.; Selzer, P.; Jacoby, E. *Curr. Top. Med. Chem.* **2005**, *5*, 751; Oprea, T. I.; Davis, A. M.; Teague, S. J.; Leeson, P. D. *J. Chem. Inf. Comput. Sci.* **2001**, *41*, 1308.
7. Blaney, J.; Nienaber, V.; Burley, S. K. In *Fragment-based Approaches in Drug Discovery*; Jahnke, W., Erlanson, D., Eds.; Wiley-VCH: Weinheim, Germany, 2006; p 215.
8. For a description of the structure of NS5b see Bressanelli, S.; Tomei, L.; Roussel, A.; Incitti, I.; Vitale, R. L.; Mathieu, M.; De Francesco, R.; Rey, F. A. *Proc. Natl. Acad. Sci. U.S.A.* **1999**, *96*, 13034; Ago, H.; Adachi, T.; Yoshida, A.; Yamamoto, M.; Habuka, N.; Yatsunami, K.; Miyano, M. *Structure* **1999**, *7*, 1417.
9. Chan, L.; Reddy, T. J.; Proulx, M.; Das, S.; Pereira, O.; Wang, W.; Siddiqui, A.; Yannopoulos, C. C.; Poisson, C.; Turcotte, N.; Drouin, A.; Alaoui-Ismaili, M. H.; Bethell, R.; Hamel, M.; L'Heureux, L.; Bilimoria, D.; Nguyen-Ba, N. *J. Med. Chem.* **2003**, *46*, 1283.
10. Chan, L.; Pereira, O.; Reddy, t. J.; Das, S. K.; Poisson, C.; Courchesne, M.; Proulx, M.; Siddiqui, A.; Yannopoulos, C. G.; Nguyen-Ba, N.; Roy, C.; Nasturica, D.; Moinet, C.; Bethell, R.; Hamel, M.; L'Heureux, L.; David, M.; Nicholas, O.; Courtemanche-Asselin, P.; Brunette, S.; Bilimoria, D.; Bedard, J. *Bioorg. Med. Chem. Lett.* **2004**, *14*, 797.
11. Each 50 μl enzymatic reaction contains 8.4 μg/mL poly-A:oligo U_{16} (template:primer), 200 nM NS5B570n-BK enzyme, 2.1 μCi of tritiated UTP (Perkin Elmer catalog No. TRK-412; specific activity: 30–60 Ci/mmol; stock solution concentration from 7.5×10^{-5} M to 20.6×10^{-6} M), 1 μM ATP, CTP, and GTP, 40 mM Tris–HCl, pH 8.0, 2–40 mM NaCl, 4 mM DTT (dithiothreitol), 4 mM $MgCl_2$, and 5 μl of compound serial diluted in DMSO. Reaction mixtures are assembled in MADVN0B 96-well filter plates (Millipore Co.) and incubated for 2 h at 30 °C. Reactions are stopped by the addition of 10% (v/v) trichloroacetic acid and incubated for 40 min at 4 °C. Reactions are filtered, washed with 6 reaction volumes of 10% (v/v) trichloroacetic acetic acid, 2 reaction volumes of 70% (v/v) ethanol, air dried, and 25 μl of scintillant (Microscint 20, Perkin-Elmer) is added to each reaction well. The amount of light emitted from the scintillant is converted to counts per minute (CPM) on a Topcount® plate reader (Perkin-Elmer, Energy Range: Low, Efficiency Mode: Normal, Count Time: 1 min, Background Subtract: none, Cross-talk reduction: Off).
12. NS5B570n-BK enzyme was minimally biotinylated and captured onto a streptavidin surface to a density of ~6000 RU. The compounds, supplied at 10 mM in 100% DMSO, were diluted in running buffer containing 50 mM HEPES, 600 mM NaCl, 10 mM $MgCl_2$, 5 mM DTT, pH 8.0, to a concentration of 5%. All compounds were run in a 3-fold dilution series using 50 mM HEPES, 600 mM NaCl, 10 mM $MgCl_2$, 5 mM DTT, 5% DMSO, pH 8.0 as the running buffer. Each compound was flowed across the HCV surface and a streptavidin control surface. For each dataset, the responses at equilibrium ($t = 60$ s) were plotted versus the compound concentration. Data points were fit to a simple binding isotherm to obtain the interaction affinity. More potent compounds exhibiting observable kinetics were fit to a 1:1 kinetic model. All data reduction and fitting was done with the Scrubber II software package (BioLogic Software, Pty., Australia).